

Experimental studies on the assessment of the bond strength and the bond stress-slip relationship have been numerous^{1,2,3,4}. The simplified bilinear t -s relationship represented in Fig.5-1 is typically suggested for analysis. The significant values of parameters that define this relationship can be evaluated using experimental results in terms of bond strength and mode II fracture energy (defined by the area under the t-s diagram). The bilinear law is given by an initial linear relationship between slip, s, and bond stress, t, up to the bond strength, t_{b1} , followed by a linearly softening branch until the maximum slip s_0 . The maximum shear stress t_1 depends on the concrete tensile strength, which can be correlated to its compressive strength.

To define the slope of the initial branch, k_1 , both the compliance of the adhesive layer (whose thickness is of the order of one millimetre) and of the concrete surface, whose deformation contributes to the interfacial slip, should be considered in terms of thickness and shear modulus.

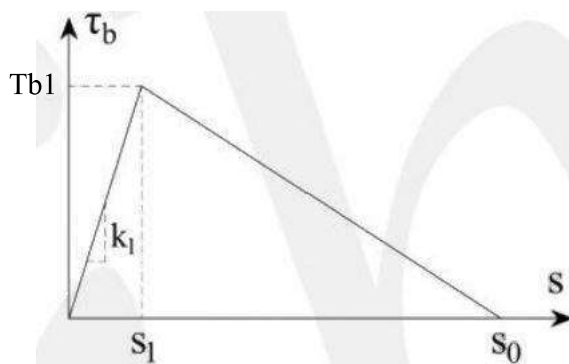


Fig.5-1 Generic bilinear t-s constitutive law for bond in EBR FRP system

The values of the maximum shear bond stress, t_1 , and ultimate slip, s_0 , depend on properties of the concrete, the strengthening system and other geometric characteristics. Some proposals for the evaluation of these parameters are reported in Appendix A5.1.1.1.

5.1.3 Bond-slip law for near surface mounted FRP

For modelling the bond behaviour of NSM FRP systems in the context of strengthening concrete structures, a local bond shear stress versus slip relationship (t-s) is also used. This relationship is affected by several parameters, among which the mechanical properties of the materials (FRP reinforcement, groove filler and concrete substrate), the surface properties of the FRP reinforcement and of the grooves, the shape of the strengthening system (bars or strips), the dimensions of the groove, the distance of the groove from the edge of the member and the depth of the FRP reinforcement into the groove^{5,6,7,8,9,10,11,12,13,14}.

Further details and references on bond of NSM and bond stress-slip relationships are reported in Appendix A5.1.2.1. Due to the large number of parameters affecting the local bond-slip behaviour of NSM reinforcements, the local bond-slip relationship for a given NSM system should be determined experimentally by selecting the most appropriate test set-up. Notably, as for EBR, also for NSM systems a simplified bilinear bond law can be assumed¹⁵.

5.2 Debonding mechanisms for EBR systems

Bond mechanisms allow transferring forces from concrete to FRP, hence bond failure modes have to be taken into account properly. In the case of EBR, bond failure occurs at the interface between the reinforcement and the concrete substrate and implies the complete loss of bond between the two materials.

Usually, debonding initiates in a limited area of the strengthened element and then propagates until the composite action is lost over a major part of the length of the FRP reinforcement. Localised debonding means a reduction of the bond performance between concrete and FRP limited to a small area, e.g., a loss in bond length a few millimetres next to a flexural or shear crack. Therefore, localised debonding is not, in itself, a failure mode that causes a significant loss of the load carrying capacity.

On the contrary, when localised debonding propagates and the composite action is lost in such a way that the FRP reinforcement is not able to carry loads anymore, bond failure is obtained. In general terms, this is also referred to as peeling-off. If no stress redistribution from the external FRP to the internal steel reinforcement is possible, peeling-off will occur as a sudden and brittle failure.

Bond failure may occur at different FRP-concrete interfaces, schematically represented in Fig.5-2 and described in the following.

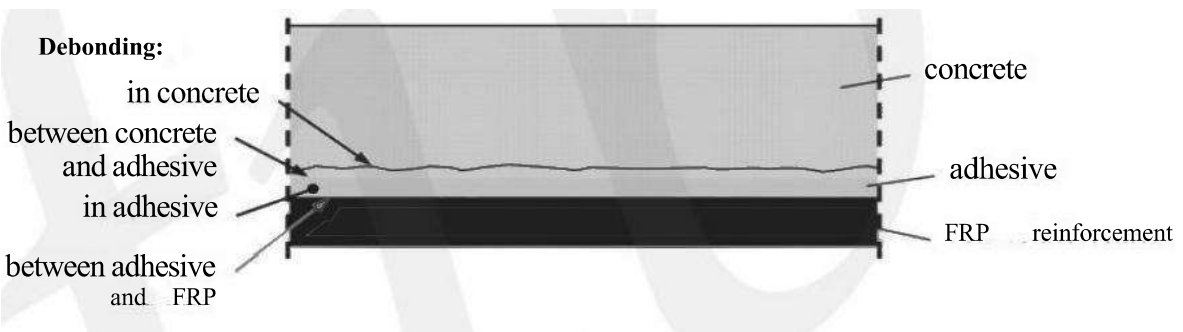


Fig.5-2 Different interfaces for bond failure

-Debonding in the concrete (cohesive failure in the concrete)

Due to the adhesive penetration into the concrete micro-structure, a thin layer of concrete in contact with the adhesive attains a higher strength, resulting in debonding along a surface parallel to the FRP, a few millimetres from the concrete surface. Moreover, debonding can occur along a weakened layer, e.g. along the line of the embedded steel reinforcement (Fig.5-3).

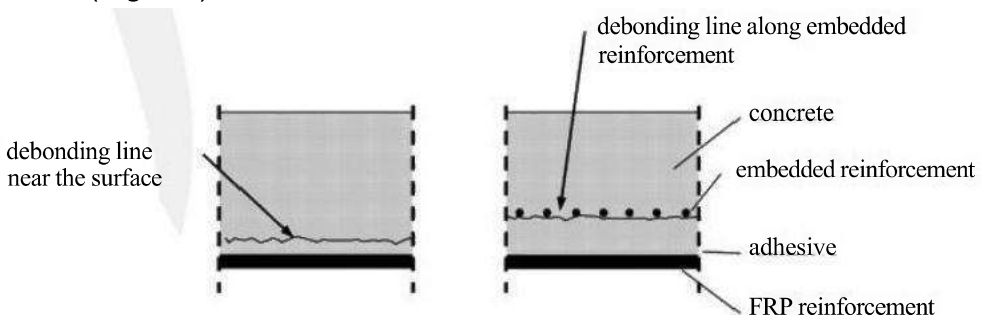


Fig.5-3 Different debonding surfaces in the concrete

-Debonding in the adhesive (cohesive failure in the adhesive)

Debonding may occur through the adhesive layer only if its strength is lower than that of the concrete(e.g.at high temperatures or when the strength of concrete is particularly high).

-Debonding at the interfaces between concrete and adhesive or adhesive and FRP reinforcement (adhesion failure)

Bond failures along the interfaces between concrete and adhesive or adhesive and FRP reinforcement may only occur if there is insufficient surface preparation before the strengthening application process,since the cohesion strength of epoxy resins is lower than the adhesion strength.

-Interlaminar shear failure in FRP

Since the FRP reinforcement is a composite material,debonding may also occur within the FRP material system.This failure mechanism initiates when the maximum shear stress in the FRP reaches its shear strength.However,typical polymer matrix materials (as structural adhesives)have shear strengths that are several times(e.g.six to eight)higher than that of concrete,so this failure mechanism is very rare,hence no further elaboration will be given hereafter.

Most bond failures observed in experimental tests on RC members flexurally strengthened with FRP materials occur in the concrete layer near the surface,generally being the weakest region in the FRP/concrete system.

5.2.1 Debonding mechanisms in RC beams with flexural strengthening

Debonding failure modes in RC beams strengthened in flexure with FRP materials can be classified on the basis of the location where debonding starts:*end debonding*, which occurs at the curtailment region of the FRP reinforcement,if it is not sufficiently anchored;*and intermediate crack debonding*,which occurs at an intermediate section along the beam by bridging flexural or flexural-shear cracks.

5.2.1.1 End debonding failure

Two types of failure modes can be generally observed at the end anchorage of beams externally strengthened with FRP materials:one is strictly related to the bond stresses along the FRP reinforcement-concrete interface (named interfacial debonding at the anchorage zone);the other is related to a shear deficiency of the RC element (named *concrete cover separation or concrete rip-off*).

Interfacial debonding at the anchorage zone is initiated by high shear and normal interfacial stresses near the end of the FRP^{16,17,18,19}.The combination of these shear and normal stresses can develop principal tensile stresses that attain the concrete tensile strength.Usually,if a correct preparation of bonded surfaces is carried out,failure occurs in the concrete since its tensile strength is lower than that of the adhesive.The debonding runs in a very thin layer of concrete adjacent to the adhesive interface,starting at the end of the FRP and running along the beam span (Fig.5-4a).

When the distance between the plate end and the adjacent beam support is small,the anchorage failure can be triggered otherwise(Fig.5-4b).Hereby,the failure is induced at the first crack intersecting the strip,with the detachment similar to what happens in shear bond tests(Fig.5-7)^{20,21,22,23,24,25,26,27,28}.

Both types of failure can be generally indicated as FRP end debonding and can be effectively avoided by adopting a proper curtailment of the FRP (Chapter 6) or by end anchorage devices, as explained in detail in Chapter 9.

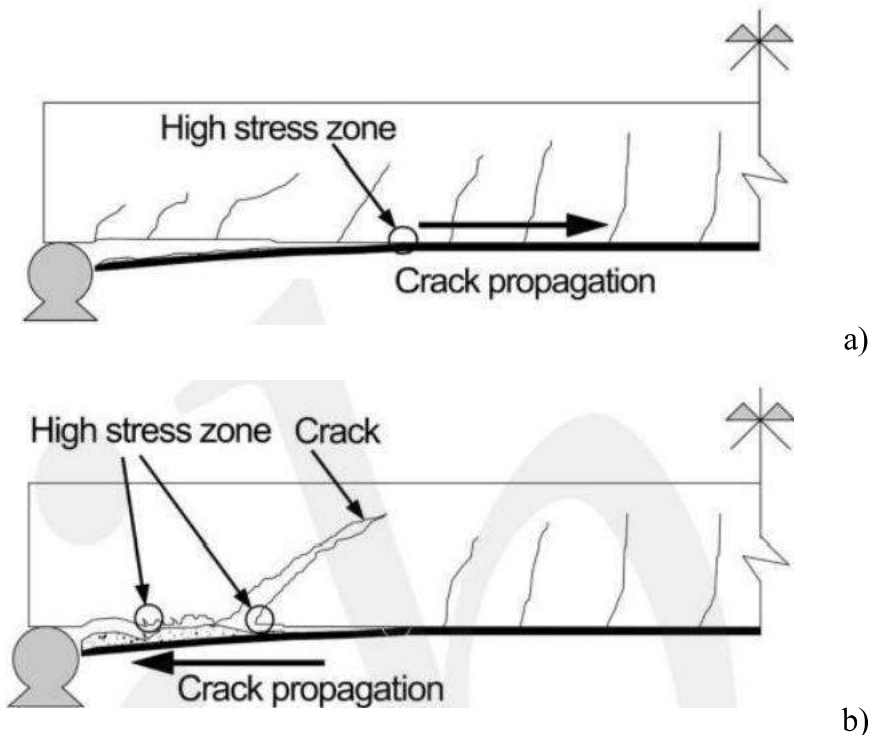


Fig.5-4 FRP end debonding:(a)interfacial debonding due to combined effects of shear and normal stresses at the FRP end;(b)interfacial debonding due to anchorage force at the first crack

Concrete cover separation (or concrete rip-off failure) involves the tearing-off of the concrete cover along the level of the steel tension reinforcement starting from the FRP end. In particular, if the end of the FRP reinforcement is subjected to a shear force with negligible or no bending moment, the debonding is mainly due to the shear force. This failure is usually associated with the formation of a critical inclined crack near or at the end of the FRP in the unstrengthened part (Fig.5-5a). In this case the concrete cover together with the FRP reinforcement may be regarded as a composite thick plate bonded to the steel tension reinforcement of the beam and subjected to high interfacial stresses when the curvature of the beam increases²⁹. The concrete rip-off failure can also be understood from the shear truss analogy (Fig.5-5b), where it can be observed that the external FRP reinforcement is not engaged by the internal shear links (missing shear tie resulting from the shift in tensile forces between the FRP and the internal rebars), as a result of which the concrete cover fails in tension and the shear crack further propagates along the level of the internal reinforcement³⁰. Hence, such a failure can be significantly suppressed by shear strengthening measures, e.g. through the use of externally bonded U-shaped FRP jackets.

Concrete rip-off failure has been commonly reported as premature failure mode in laboratory tests^{31,32,33,34}. Since the bond failure of the FRP reinforcement is induced by the appearance of a shear crack, such failure is sometimes also classified as end shear debonding³⁵ or critical diagonal crack debonding with concrete cover separation³⁶. A variety of strength models have been proposed^{36,37,38,39,40,41,42}, mainly based on shear force verification or on a combined shear-moment verification at the end section of the FRP reinforcement.

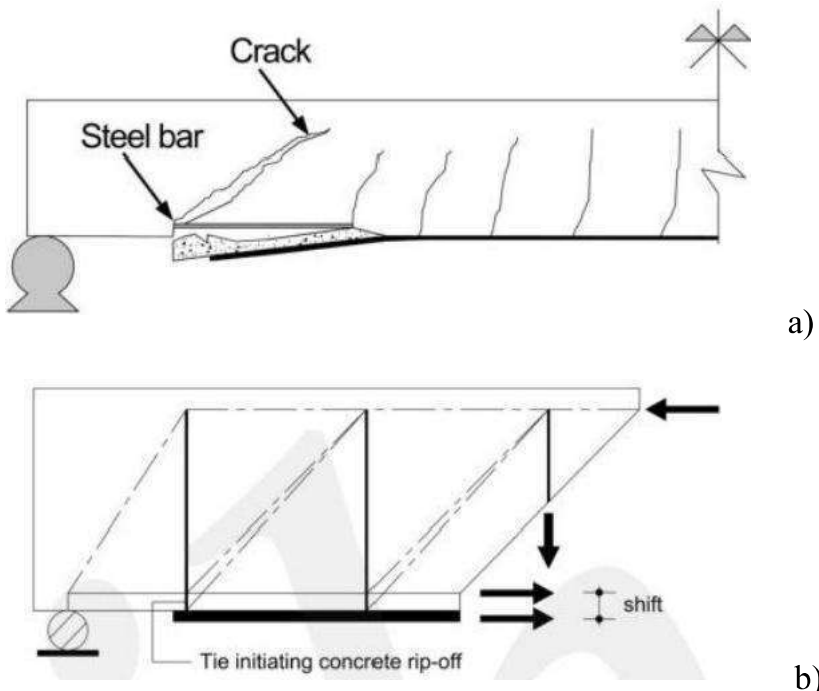


Fig.5-5 Debonding by concrete cover separation:(a)induced by a critical diagonal crack close to the FRP end,(b)due to the missing shear tie resulting from the shift between tensile forces

5.2.1.2 Debonding at intermediate cracks

In RC elements externally strengthened in flexure with FRP materials, debonding can also occur at intermediate flexural (Fig.5-6a) or shear-flexural cracks (Fig.5-6b) away from the ends of the FRP reinforcement, due to the effect of the bond shear interfacial stresses. Such debonding then propagates towards the end (Fig.5-6)^{30,32,34,41,43,44}. The failure occurs in the concrete with the detachment of a thin layer due to the predominance of bond shear stress effects. This failure mode is usually indicated as intermediate crack debonding (IC debonding) in the case of Fig.5-6a and critical shear crack debonding (CDC debonding) in the case of Fig.5-6b. Indeed, the formation of a critical crack can be influenced by the loading pattern, resulting in a combination of horizontal and vertical crack opening, bridged by the FRP and initiating the debonding. As has been observed in many experimental tests where a concentrated load is applied^{5,30,45} (Fig.5-6b), the critical crack often occurs in regions with a combination of high moments and shear forces, resulting in a steep critical shear-flexure crack for which the vertical crack opening is less arrested by the internal stirrups.

5.2.2 Debonding due to unevenness

Small unevenness of the concrete surface, especially concave shaped, may cause phenomena of local debonding of the FRP reinforcement, but this is unlikely to cause complete debonding. However, a proper treatment of the concrete surface to remove dust, unevenness, dirt, oil, etc. with sand-blasting or similar procedures and to fill voids and cracks, should be followed in order to improve the bond between the adherent materials and mitigate the risk of local debonding (see Section 10.3.2.1 for more details).

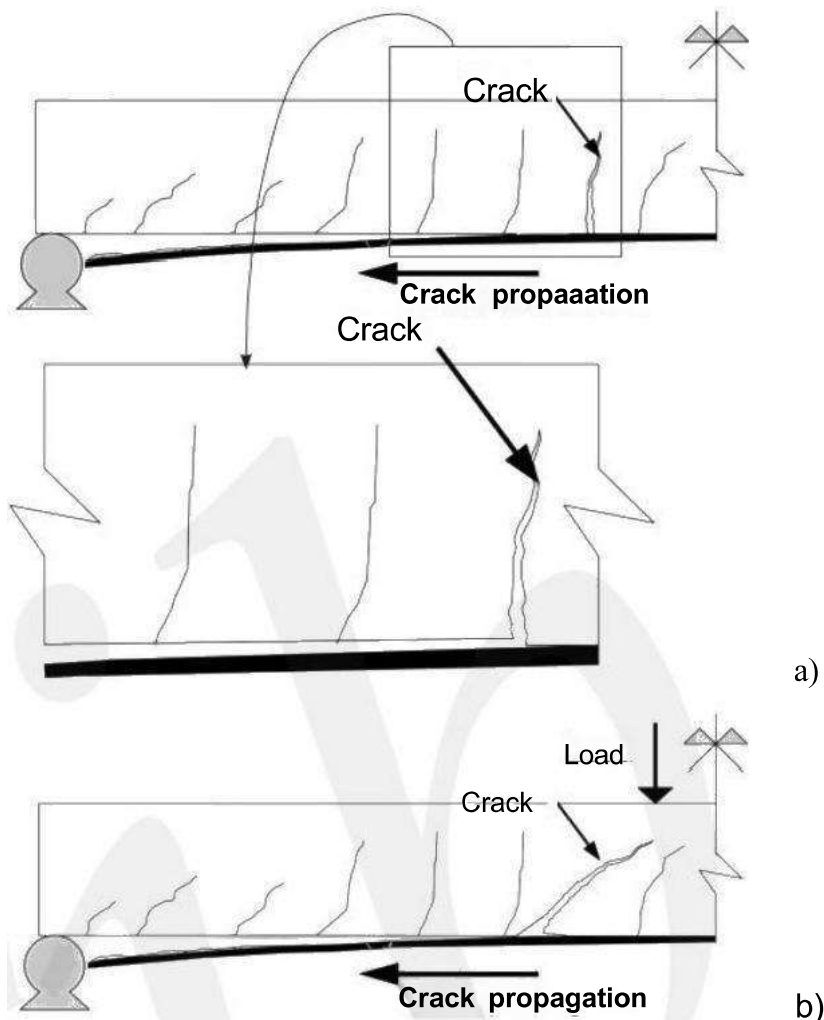


Fig.5-6 Debonding at (a) an intermediate flexural or (b) flexural-shear crack

5.3 Safety verifications with respect to debonding of EBR systems

5.3.1 Effective bond length

The safety verification for debonding failure requires, in general, the evaluation of the maximum tensile stress that may be carried by the external FRP and, thus, the maximum transferable stress to the concrete support.

With reference to a typical bond test, such as schematically represented in Fig.5-7, the maximum value of the force in the FRP strengthening, F , (equal to the FRP stress F_0 times its cross-sectional area) depends on the length l_0 of the bonded area. F increases with l_0 up to a maximum value corresponding to a certain length l_e , beyond which the transmitted force remains practically constant. The length l_e is named effective bond length and corresponds to the minimum bonded length capable of ensuring the transfer of the maximum force between the concrete element and the external FRP reinforcement⁴⁶. In particular, with reference to a generic T-s bond law (e.g. Fig.5-1) characterised by a softening branch leading to an ultimate slip s_u (corresponding to an almost null residual shear stress), the effective length is the bonded length necessary to attain s_u at the loaded section of the FRP reinforcement in a bond test.

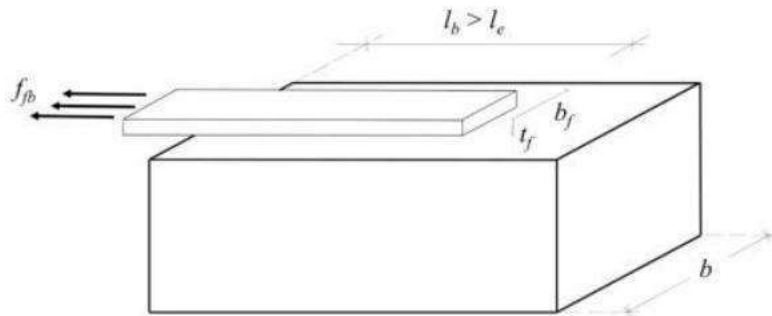


Fig.5-7 Maximum stress transmitted by FRP strengthening in the case of bonded length longer than the effective length

Solving the differential equation of bond under the simplified assumption of a rigid-softening bilinear law ($s_i=0$ in Fig.5-1) and considering the boundary values at the end anchorage, the effective bond length l_e is obtained as:

$$l_e = \frac{\pi}{2} \sqrt{\frac{E_f \cdot t_f \cdot s_0}{\tau_{b1}}} \quad (5-3a)$$

From Eq.(5-3a) it is concluded that/depends on the stiffness of the FRP system (thickness, t_f , and elastic modulus in the loading direction, E_f), on the deformation capacity of the system (s_0) and on the bond strength τ_{b1} (see Fig.5-1).

Under the assumption of a bilinear bond law, Eq.(5-3a) can be rewritten as follows:

$$l_e = \pi s_0 \sqrt{\frac{E_f \cdot t_f}{8G_f}} \quad (5-3b)$$

where G_f is the fracture energy, defined as the area under the bond-slip curve:

$$G_f = \frac{\tau_{b1} \cdot s_0}{2} \quad (5-4)$$

In general, for whatever t_f - s relationship, the fracture energy depends on the strength properties of the concrete and the adhesive and on the characteristics of the concrete surface. In particular, if the FRP reinforcement is correctly applied, debonding occurs in the concrete and the fracture energy can be expressed as a function of the bond strength, τ_{b1} . Since t_f depends on the concrete tensile strength, the fracture energy can be directly expressed as a function of the mean tensile, f_{ctm} , or mean compressive, f_{cm} , strength of concrete:

$$G_f = G_f(f_{ctm}) \quad G_f = G_f(f_{cm}) \quad (5-5a)$$

This assumption is quite reliable in the case of a simple shear bond test.

The following general expression can be adopted for the fracture energy assuming a direct dependence on the mean compressive strength of concrete:

$$G_f = k^2 \cdot k_b^2 \cdot f_{cm}^{2/3} \quad (5-5b)$$

where the shape factor k , (≥ 1) is defined as follows:

$$k_b = \sqrt{\frac{2 - b_f/b}{1 + b_f/b}} \quad (5-6)$$

where b_e and b_s is the width of the external FRP reinforcement and of the strengthened element, respectively (see Fig.5-7).

Thus, the effective bond length / may be estimated from the following general expression:

$$l_e = \frac{\pi s_0}{k_b \cdot k} \sqrt{\frac{E_f \cdot t_f}{8f_{cm}^{2/3}}} \quad (5-7a)$$

The coefficient k has to be calibrated by a statistical procedure. In particular, assuming $s_0=0.25$ mm, the values of the coefficient k can be taken equal to 0.25 or 0.17 for mean value and 5% characteristic value, respectively (see Section 5.3.2.3 for more details). Thus, the effective bond length / may be written as:

$$l_e = \frac{\pi}{k_b} \sqrt{\frac{E_f \cdot t_f}{8f_{cm}^{2/3}}} \quad \text{for mean value} \quad (5-7b)$$

$$l_e = \frac{0.25\pi}{0.17k_b} \sqrt{\frac{E_f \cdot t_f}{8f_{cm}^{2/3}}} \approx 1.5 \frac{\pi}{k_b} \sqrt{\frac{E_f \cdot t_f}{8f_{cm}^{2/3}}} \quad \text{for 5% characteristic value} \quad (5-7c)$$

5.3.2 Ultimate strength for debonding at the end anchorage zone

In order to prevent end debonding both peeling-off at the anchorage zone and cover separation should be verified. For the latter, reference is made to Appendix A5.1.1.4 and Section 6.3.5. For the former, the bond behaviour at the end of the reinforcement can be considered similar to what happens in bond tests (Fig.5-7) to verify the FRP anchorage capacity as a function of bond length.

5.3.2.1 FRP anchorage capacity

In EBR-strengthened concrete elements the bond behaviour at the anchorage zone (Fig.5-4) can be simulated by what happens in bond tests, if the interfacial shear stresses are predominant and, thus, the normal stresses can be considered negligible. Based on this assumption and by means of fracture mechanics, several formulations have been proposed in the past years to perform safety verifications for debonding at the end anchorage zone [22, 25, 42, 47, 48, 50, 51]. Most of these formulations have a theoretical approach and numerical coefficients derived from statistical regression analysis of experimental results of bond tests. The general expressions of the maximum tensile stress, f_{tb} , and of the tensile force in the FRP at debonding, F_{tb} , are:

$$f_{tb}(l_b) = \beta_l(l_b) \sqrt{\frac{2E_f \cdot G_f}{t_f}} \quad (5-8a)$$

$$F_{tb}(l_b) = \beta_l(l_b) b_f \sqrt{2E_f \cdot t_f \cdot G_f} \quad (5-8b)$$

where β_l is a factor that depends on the bond length according to the following equation:

$$\beta_l = \begin{cases} \frac{l_b}{l_e} \left(2 - \frac{l_b}{l_e} \right) & \text{if } l_b < l_e \\ 1 & \text{if } l_b \geq l_e \end{cases} \quad (5-9)$$

Bond lengths, I_b , shorter than the effective one, I_e , so that $\beta < 1$, may occur, for instance, in shear strengthening.

5.3.2.2 Solution with the bilinear bond stress-slip relationship

Under the assumption of bilinear bond law (Fig.5-1), the fracture energy can be expressed by Eq.(5-4) and, thus, Eq.(5-8a) for the maximum stress in the FRP at debonding becomes:

$$f_{ib}(I_b) = \beta_l(I_b) \sqrt{\frac{E_f \cdot s_0 \cdot \tau_{bl}}{t_f}} \quad (5-10)$$

Some indications about the calculation of the mean and characteristic values of the bilinear bond law are reported in Appendix A5.1.1.1.

5.3.2.3 Solution based on "design by testing" approach

With respect to debonding at the end anchorage zone, the mean, the 5% characteristic and the design debonding strength, f_{ibm} , f_{ibk} and f_{ibd} in the FRP reinforcement can be calculated by means of Eq.(5-8a) introducing Eq.(5-5b) for the fracture energy:

$$f_{ibm} = k_m \cdot k_b \cdot \beta_l \sqrt{\frac{2E_f f_{cm}^{2/3}}{t_f}} \quad [\text{forces in N, lengths in mm}] \quad (5-11)$$

$$f_{ibk} = k_k \cdot k_b \cdot \beta_l \sqrt{\frac{2E_f f_{cm}^{2/3}}{t_f}} \quad [\text{forces in N, lengths in mm}] \quad (5-12)$$

$$f_{ibd} = \frac{k_k}{\gamma_{ib}} k_b \cdot \beta_l \sqrt{\frac{2E_f f_{cm}^{2/3}}{t_f}} \quad [\text{forces in N, lengths in mm}] \quad (5-13)$$

where the partial factor $\gamma_m=1.5$ (see Section 3.6.3).

The numerical coefficient k can be calibrated by a statistical procedure as the least-square coefficient minimizing the difference between theoretical values and experimental results according to the design by testing philosophy to determine capacity models suggested in EN 1990⁵². For surface bonded CFRP and the data set range as reported in Appendix A5.1.1.3, this procedure⁵³ yields $k=0.25$. Moreover, under the hypothesis that the debonding load has a normal distribution⁵⁴ the lower characteristic value of the bond strength can be obtained⁵⁵ considering the 5% characteristic value of the parameter k as $k=k_0/0.5=0.17$.

The tensile force in the external reinforcement can be calculated using Eqs(5-11),(5-12) or(5-13) multiplied by the area of the external reinforcement b_t .

5.3.3 Ultimate strength for debonding at intermediate cracks

In order to prevent debonding failure at intermediate cracks and considering successive levels of approximation⁵⁵, two main approaches can be used: (a) a simplified FRP stress limit approach based on the maximum strain in the FRP (Section 5.3.3.1 and Section 6.2.1.3.1) and (b) a more accurate approach based on the bond force transfer at the concrete elements between cracks (Section 5.3.3.2 and Section 6.2.1.3.2). Other approaches are possible, such as the one based on bending-shear interaction (see Appendix A6.2) or the one based on the shear transfer between the concrete and external FRP reinforcement (see Appendix A6.3).

5.3.3.1 Simplified approach based on maximum strain in the FRP reinforcement

According to the simplified FRP stress limit approach, at the ultimate limit state the maximum bending moment in a flexurally-strengthened member can be calculated assuming that in the FRP reinforcement the tensile stress does not exceed the lower fractile(5%) value of the bond strength, $f_{bd,IC}$ obtained by the corresponding mean value, $f_{bd,m}$, by applying the following equations:

$$f_{bd,m} = k_m f_{bd,m} \quad (5-14)$$

$$f_{BK,JC} = k_k f_k \quad (5-15)$$

$$f_{bd,IC} = \frac{f_{bd,k,JC}}{\gamma_{fb}} \quad (5-16)$$

where the mean and characteristic values of the bond strength, f_m and f_K , are defined by Eqs.(5-11) and (5-12), respectively, considering $\beta_1=1$. The coefficients $k_{ct,m}$ and k_{ck} can be taken equal to 2.1 and 1.8, respectively, if no specific data are available (see Appendix A5.1.1.5). The safety factor can be assumed 1.5.

Equations (5-14) and (5-15) are based on those proposed for the maximum stress in the FRP in case of end debonding, corrected by a coefficient $k>1$. This is because the interfacial shear stresses relate to the FRP force gradient along the length of the beam, rather than the anchorage capacity at the FRP end. This implies that the value of the maximum FRP strain related to the intermediate crack debonding can be assumed higher than that pertaining to end debonding.

The corresponding value of the design strain in the FRP reinforcement, $\epsilon_{bd,IC}$ is:

$$\epsilon_{bd,IC} = \frac{f_{bd,IC}}{E_f} \quad (5-17)$$

This limiting value of strain in the FRP reinforcement should be adopted in the critical sections of the strengthened element, i.e. in the sections where the bending moment is maximum and where it is assumed that a flexural or shear/flexural crack will form. More details about this and about the calculation of the resisting bending moment of the strengthened section are given in Chapter 6.

5.3.3.2 Approach based on the bond force transfer at the concrete elements between cracks

According to this approach, the stress variation, Δo , in the FRP between two adjacent cracks should not exceed a suitable limiting value Δo , which corresponds to the maximum increase in tensile stress that can be transferred by means of bond stresses along the crack spacing. The value of Δo depends, in general, on the bond constitutive law, on the distance between cracks, s , and on the stress level, o , in the FRP reinforcement under the ultimate load condition^{35,56,57}.

The formulation given in DAfStb (2012)⁵⁷, and as presented in Section 6.2.1.2.2, is based on the definition of the bond shear strength and includes the effect of the bond of the external reinforcement, the bond friction and the element curvature.

5.3.4 Effect of fatigue

The effect of fatigue on bond behaviour of RC elements strengthened with EBR is not fully understood, mainly due to difficulties in applying cyclic loading, especially with sign changes. According to tests on beams, fatigue damage has been shown not to be significant if the FRP-strengthened RC member is exposed to typical service load ranges (roughly between 30% and 60% of the load required to induce first yield), but damage can occur if the load range exceeds 60% of the load at first yield⁵⁸. Bending tests with a low number of cycles considering different load levels, among which in proximity of internal steel yielding (hence beyond 60% of the yield load) were carried out by Ceroni⁵⁹. These indicate a slight reduction, in the order of 10%, of the bond strength. Reversed cyclic loading may result in buckling of the FRP, which could reduce the bond strength^{59,60,61}. In general, the bond strength is not affected by fatigue as long as stresses and slip are in the linear elastic part of the stress-slip curve. Fatigue verifications are described in detail in Chapter 6.

5.4 Debonding mechanisms for NSM FRP systems

5.4.1 Debonding mechanisms

Bond tests on concrete elements strengthened with NSM FRP bars or strips performed by several researchers^{5,6,8,10,49,62,63,64} evidenced different types of failure modes depending mainly on bonded length, surface configuration and a shape factor, k , defined in Fig.5-8 according to the type of NSM system (round bar, square bar, strip).

Another geometrical shape factor can be defined as the ratio of the perimeter to the area of the cross section, p/A . In general, the higher this ratio the higher the effectiveness of the NSM system in terms of bond performance^{15,49}. The material and geometric properties of the FRP play also an important role on the bond behaviour, since higher values of p/A , E , lead to stiffer bond connections.

The possible failure modes are: (a) debonding at the FRP-epoxy interface; (b) debonding at the epoxy-concrete interface; (c) epoxy cover splitting; and (d) concrete cover splitting. These failure modes are briefly described below along with the underlying failure mechanisms.

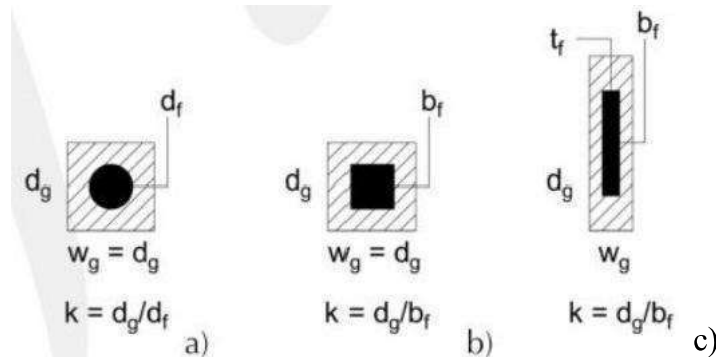


Fig.5-8 Definition of shape factor for (a) round NSM bars, (b) square NSM bars and (c) rectangular NSM strips

-Failure at the FRP-epoxy interface

This mode occurs as either pure interfacial failure (Fig.5-9a) or as cohesive shear failure in the epoxy (Fig.5-9b). The pure interfacial mode is critical for bars with a

smooth or lightly sand-blasted surface⁴, i.e. when the bond resistance relies primarily on adhesion between the bar and the epoxy. This type of failure is identified by the virtual absence of adhesive attached to the bar surface after failure. For round bars, longitudinal cracking of the epoxy cover produced by the radial components of the bond stresses may accelerate the occurrence of an interfacial failure.

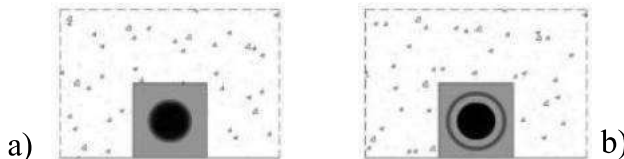


Fig.5-9 Failure at the bar-epoxy interface:(a)interfacial failure;(b)cohesive shear failure in the epoxy⁰

The cohesive shear failure of the epoxy was observed for strips with a roughened surface⁶, as well as with smooth surfaces especially when the bond length was less than the effective bond length⁸⁴⁹. Note that the effective bond length is limited by the tensile strength of the concrete cover and it increases with the elastic modulus of the FRP system. Thus, in order to obtain failure at the FRP-epoxy interface, the bond length should be lower than the effective length for FRP systems of relatively high elasticity modulus (e.g. with carbon or aramid fibres and structural adhesives with elastic modulus higher than about 4 GPa).

This type of failure is identified by the presence of adhesive on both the FRP and the concrete after debonding and occurs when the tensile strength of the epoxy is reached. In particular, it is caused by the much higher tensile stresses in the adhesive than in the surrounding concrete. Since the surrounding concrete is much stiffer than adhesives, it introduces some confinement at the concrete-adhesive interface. Therefore, according to the Mohr-Coulomb principles a pure sliding failure mode at the concrete-adhesive interface is avoided and failure is induced within the adhesive.

If the bond length is longer than the effective one, this type of failure is quite rare with structural adhesives typically used in practice.

-Failure at the epoxy-concrete interface

Bond failure at the epoxy-concrete interface may occur as pure interfacial failure (Fig.5-10a) or as cohesive shear failure in the concrete (Fig.5-10b). The interfacial failure mode was found to be critical for precast grooves⁶², which is not the case in practice, and in general for grooves with smooth surfaces. Indeed, in this case the internal friction angle of the materials in contact is quite limited and therefore the shear strength at the interface (due to the Mohr-Coulomb effect) is low and as such it becomes the weakest link of the system.

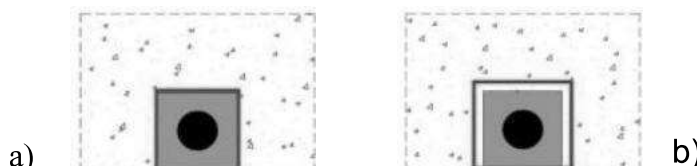


Fig.5-10 Failure at the epoxy-concrete interface:(a)interfacial failure¹⁰;(b)cohesive shear failure in the concrete¹⁵

For grooves with rough surface and with a large enough bonded length, the cohesive shear failure in the concrete is the most common failure mode¹⁵, since the lowest strength activated

in the bond mechanism is the tensile strength of the concrete surrounding the groove. This failure mode has been observed also in bond tests on concrete specimens strengthened with smooth NSM strips^{49,63}.

In general, failure at the epoxy-concrete interface was experimentally observed for values of the shape factor $k > 1.5-2.01^{\circ}$.

-Epoxy cover splitting

Longitudinal cracking of the groove epoxy filler accompanied (Fig.5-11a) or not (Fig.5-11b) by fracture of the surrounding concrete along inclined planes can occur and is generally identified as cover splitting. This was observed to be the critical failure mode for deformed (i.e. ribbed and spirally wound) round bars in moderate strength concrete^{5,65}.



Fig.5-11 Epoxy splitting failure:(a)splitting of epoxy cover and fracture of concrete along inclined planes; (b)splitting of epoxy cover without cracking of concrete¹⁰

Specimens with low values of groove size ($k \approx 1$) and very brittle adhesives can show splitting of the epoxy paste without significant damage in the surrounding concrete. By increasing groove depth and epoxy thickness, the resistance of the epoxy cover to splitting increases and failure is controlled by cracking of the surrounding concrete. In these cases the bond strength can also increase with the groove size until the failure load corresponding to the epoxy-concrete interface failure is attained. Moreover, as the FRP installed into the groove becomes deeper, the confinement introduced to the FRP from the surrounding concrete becomes higher, resulting in beneficial effects in terms of bond strength⁶.

A minimum value of $k=1.5$ is suggested to avoid splitting⁵. Splitting failure is also typical of specimens strengthened with cement-filled grooves for low values of the k factor, due to the lower tensile strength of the cement filler with respect to epoxy.

The mechanism of epoxy splitting in NSM systems is similar to splitting phenomena in the concrete surrounding deformed steel bars. The radial component of the bond stresses generates circumferential tensile stresses in the epoxy cover that may lead to the formation of longitudinal splitting cracks. The concrete surrounding the groove is also subjected to tensile stresses and may eventually fail when its tensile strength is reached, causing fracture along inclined planes. Whether fracture in the concrete occurs before or after the appearance of splitting cracks in the epoxy cover or even after the complete fracture of the cover, depends on the groove size and the tensile strengths of the two materials¹⁰.

Figure 5-12 shows schematically the bond mechanism of an NSM system in the plane perpendicular to the FRP axis. The figure also clarifies the difference in bond mechanism between strips and round bars. In the former case the normal component of the bond stresses is transverse to the thicker sides of the groove⁶, while in the latter it is circumferential; hence, splitting failure is less likely to occur in the case of strips.

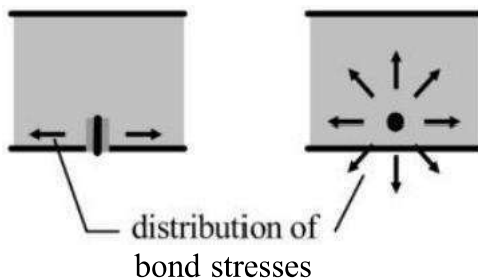


Fig.5-12 Schematic bond stress distribution in NSM strips and round bars in the plane perpendicular to the longitudinal axis of the reinforcement⁶

-Concrete cover splitting

The bond failure modes discussed above are referred to an NSM bar/strip located centrally in a wide member, where edge effects are negligible. On the contrary, when an NSM bar/strip is close to the edge of a concrete member, failure can involve the splitting of the edge concrete (Fig.5-13 67,68). This type of failure mode can be easily eliminated by keeping a minimum distance from the edge (for more details see Chapter 9, Section 9.3.2.4). Moreover this type of failure can be quite common in elements of relatively low concrete strength.

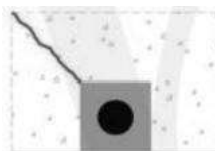


Fig.5-13 Fracture of the concrete edge⁶

5.4.2 Debonding mechanisms in beams strengthened in flexure

The likelihood of a debonding failure in a RC beam strengthened in bending with NSM reinforcement depends on several parameters, among which the internal steel reinforcement ratio^{69,70,71}, the NSM reinforcement ratio, the cross-sectional shape and the surface configuration of the NSM reinforcement, the tensile strengths of both the epoxy and the concrete and the load pattern¹⁵. Some researchers⁷² extended the NSM FRP reinforcement over the beam supports to simulate anchorage in adjacent members. Despite this anchorage, debonding failures can still occur in other locations.

There is still limited understanding of the mechanics of debonding in beams strengthened with NSM systems, even if such systems are less sensitive to debonding phenomena compared with the EBR technique. However, based on the available experimental evidence, the possible failure modes of beams flexurally-strengthened with NSM FRP reinforcements are as described below.

5.4.2.1 Interfacial debonding

Debonding at the bar-epoxy interface at the anchorage zone has been observed for sand-blasted round bars³; cohesive shear failure in the concrete has been observed starting from the cut-off section in beams with strips having a limited embedment length⁷⁴.

In general, interfacial debonding failures are similar to failures observed in bond tests on the same type of bars (see Section 5.4.1). However, unlike in a bond test, in flexural tests on beams the epoxy cover can be intersected by flexural cracks that, damaging the epoxy, could facilitate

the interfacial debonding or the epoxy cover splitting. Moreover, the loading pattern, which influences the distribution of bending moment and shear along the strengthened element, determines also if the debonding occurs at the anchorage or at an intermediate crack.

5.4.2.2 Concrete cover separation

In many tests^{67,73,75,76} bond cracks inclined at approximately 45° to the beam longitudinal axis formed on the soffit of the beam. Upon reaching the edges of the beam soffit, these cracks may propagate upwards on the beam sides maintaining a 45° inclination within the cover thickness, and then propagate horizontally at the level of the steel tension reinforcement. Debonding may occur in various modes, depending on the subsequent evolution of the crack pattern. Concrete cover separation is more probable to occur with the decrease of the distance between FRP reinforcements and with the decrease of the tensile strength of the concrete cover, due to the group effect^{69,77}.

(a) Strip end cover separation

If the NSM FRP reinforcement is terminated at a significant distance from the supports, separation of concrete cover typically starts from the cut-off section and propagates inwards^{67,69,76,78}, Fig. 5-14. This mode is similar to the concrete cover separation observed in RC beams strengthened with FRP EBR systems (see Section 5.2.1).



Fig. 5-14 Strip end cover separation⁷

(b) Localised cover separation

Cracks in the cover due to the transfer of bond stresses between the NSM reinforcement and the concrete element within or close to the maximum moment region joined with pre-existing flexural and/or flexural-shear cracks may isolate triangular or trapezoidal concrete wedges, of which one or more may eventually split off^{69,78}, resulting in localised cover separation.

(c) Flexural crack-induced cover separation

Separation of the concrete cover can occur in the location of flexural cracks almost simultaneously over a long portion of the NSM reinforcement, often involving one of the shear spans and the maximum moment region⁷³. This mode is similar to the failure induced by an intermediate crack observed in RC beams with EBR FRP (see Section 5.2.2).

(d) Flexural-shear crack-induced cover separation

As in the EBR technique, the shear sliding and the crack opening movements of a flexural-shear critical crack can promote the concrete cover separation^{78,79}, Fig. 5-15.

When NSM FRP strips with a high moment of inertia are used, longitudinal fracture along the strip may be observed, which contributes to the premature detachment of the FRP reinforcement^{78,79}, Fig.5-16.



Fig.5-15 Concrete cover separation due to the propagation of a flexural shear failure crack⁷⁸



Fig.5-16 Fracture along the strip⁷⁸

(e) Beam edge cover separation

When the NSM FRP bars are located near the edges, detachment of the concrete cover along the edges may occur.

5.4.3 Debonding mechanisms in beams strengthened in shear

In case of NSM used for the shear strengthening of RC beams, apart from the bar-epoxy and the epoxy-concrete bond failure modes, another failure mode has been observed, designated as "concrete cone failure". This failure is characterised by cone-shaped spalling of the concrete surrounding the FRP bars/strips, originating along the embedded length of the FRP and propagating towards the external surface of the concrete (see Fig.5-17a^{80,81}, Fig.5-17b⁸²).

When the spacing between FRP reinforcements is small and/or the concrete strength of the beam is low, detachment of the concrete cover from the beam core may occur due to the interaction among the FRP elements^{80,81,82}, Fig.5-17b.

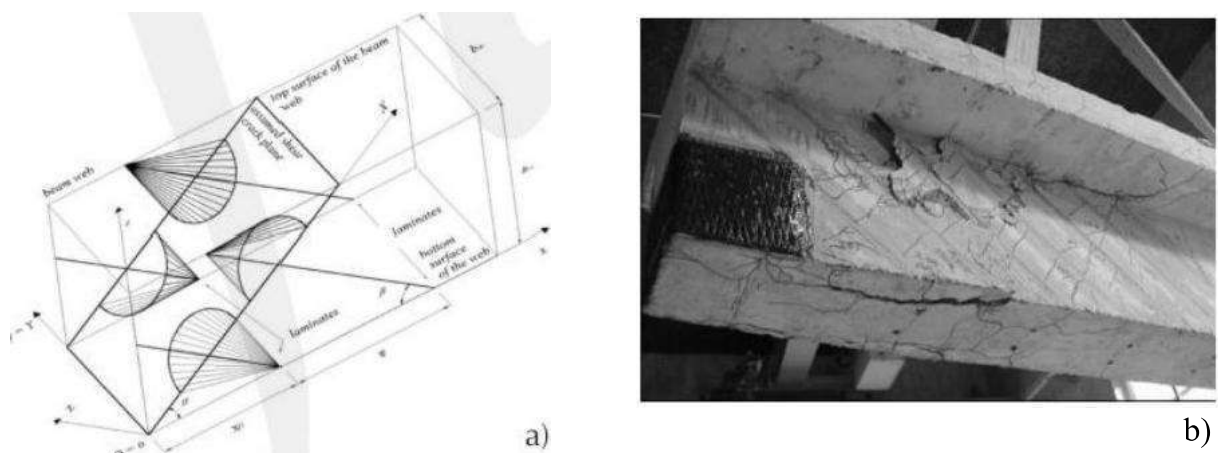


Fig.5-17 Concrete cone failure mode in NSM shear strengthening:(a)concept;(b)detachment of the concrete cover from the beam's side

According to available experimental data, the pull-out force of NSM reinforcement of rectangular cross section depends on the available bond length. For values of bond length

up to 200 mm the prevailing failure mode is concrete semi-conical fracture, for values between 200 mm and 300 mm the failure mode is debonding and for values higher than 300 mm the failure mode involves tensile rupture of the FRP. Due to interaction of concrete semi-conical fracture surfaces when the distance s , between consecutive NSM bars/strips is smaller than a critical value, a failure mode characterised by the progressive detachment and outward expulsion of the concrete cover from the underlying beam core can occur⁸³, Fig.5-18. However, parametric studies on the influence of s , on the shear contribution of NSM strips evidenced that the group effect is only significant for very small values of s , not practically applicable due to economic reasons^{81,83}.



Fig.5-18 Expulsion of the concrete cover

5.5 Safety verifications with respect to debonding of NSM systems

5.5.1 Bond length

In general, the ultimate load increases for higher bonded lengths both for round bars and for strips⁷³.

Similar as defined in Section 5.3.1, the effective bond length, I , can be defined as the length corresponding to the minimum bonded length needed to ensure the transmission of the maximum anchorage force, which is achieved with the full development of the bond law (reaching an ultimate slip in the NSM with zero shear stress). A higher bonded length does not increase the transmitted force. According to test results⁵, a bonded length of 300 mm was sufficient for the NSM FRP system to develop fully the bond stress-slip law.

If the tensile stress in the NSM FRP reinforcement reaches its tensile strength before debonding, the full capacity of the reinforcement can be developed. The corresponding value of the bond length is usually named development length, I_b ⁶⁵. The available experimental data show that, unlike for externally bonded reinforcement, a development length may exist for NSM systems due to the larger ductility of their local bond behaviour. This is especially the case for NSM strips, which in laboratory tests have developed their full tensile capacity⁸. One study⁶ estimated this length as approximately 150 mm (15 times the strip width) in absence of edge effects (net edge distance ≥ 75 mm), when relatively thin strips were used. For thicker NSM strips the development length could increase⁷⁶

5.5.2 Ultimate strength for debonding

For NSM FRP reinforcements, no general formulae can yet be provided to determine the debonding failure load associated to any given bond length, due to the large number of parameters affecting the local bond-slip behaviour and of types of NSM systems available in the market. Therefore, reference is made to the following two tentative

provisions to assess the anchorage force:(1)based on the minimum bond strength of the concrete and the adhesive⁵⁷,as provided in Section 6.2.2.3;and (2)based on statistical regression analysis of bond test data⁸⁴,as provided in Appendix A5.1.2.2.

In general,once the local bond-slip relationship for a given NSM system is determined experimentally and the corresponding equation is found,the failure load can be determined as a function of the bond length by solving the differential equation of bond.In any case the strength of the system depends on the type of failure,i.e.the fracture energy depends on the failure surface type and dimension(at the bar-epoxy interface,at the epoxy-concrete interface,in the concrete).As for the case of the EBR system,the general expression for the maximum tensile stress in the FRP reinforcement at failure can be written as:

$$f_{rb} = \sqrt{\frac{2E_f \cdot G_f \cdot p_f}{A_f}} \quad (5-18)$$

where G_f is the fracture energy associated to the interfacial bond law and p and A_f the perimeter and the area of the cross section of the NSM FRP reinforcement,respectively.

In the case of epoxy cover splitting,the local bond strength increases with the depth of the groove.

For interface failure modes,the tensile strength of concrete becomes a relevant parameter influencing the failure load¹⁰.

The maximum load is higher for rough grooves than for smooth ones,due to the more ductile bond behaviour provided by the former surface conditions.In case of interface failure,for a fixed cross section,the maximum load increases with the elastic modulus of the FRP system and in general increases with the axial stiffness and the surface roughness of the NSM system¹⁵.

Strips can show a better behaviour compared with round bars with similar axial stiffness in terms of ductility and maximum load.In particular,the favourable effect of the rectangular shape of the cross-section of the strips can be explained by the larger bond perimeter and the high degree of confinement provided by the surrounding concrete⁷⁷.

When smooth NSM carbon strips are installed in a deeper position inside the grooves,a higher failure load is obtained due to the more effective confinement provided by the surrounding concrete to the strips^{49,85}.

Finally,in cases where the NSM reinforcement is needed over the entire length of a member,it can be easily anchored to adjacent members in order to prevent debonding failure at a cut-off section.

5.5.3 Effect of fatigue

Tests involving fatigue loading histories have evidenced that the bond strength of NSM strips is not significantly diminished as long as the upper load level of each cycle does not exceed 60%of the debonding load for monotonic conditions and a stress amplitude of 250 MPa in the strip is not exceeded^{67,86}.

Experimental results of cyclic pull-out bending tests with unloading/reloading cycles at 60%,75%and 90%of the maximum force without sign reversals⁸⁷evidenced that:the monotonic load-slip relationship envelopes the cyclic response curves;in the unloading/reloading cycles the peak load decreased at the end of the reloading branches,i.e.a

stiffness degradation occurred; and the debonding failure load was not influenced by the cyclic loading.

Based on this knowledge and the existing limits for the stress amplitude of internal steel reinforcement, it is deduced that the bond performance of NSM strips is not critical for the bond behaviour under fatigue loading.

5.6 Mechanical anchorages

Debonding at the ends of surface bonded FRP systems can be avoided, or an enhancement of the debonding failure load can be achieved, using anchorage systems. Various solutions are available and can be designed for the specific case employing the fibres themselves with suitable configurations or additional devices such as bolts, plates, fibre fans, etc.

Details about anchorage systems, their efficiency and specific aspects are discussed in Chapter 9. In any case when special anchorage devices are used, the maximum tensile stress in EBR FRP reinforcements should be evaluated through special experimental investigations and should not be taken higher than 90% of the design tensile strength of FRP (see also Section 6.2.1.3.4).

As a result of a strap enclosure at the ends of FRP used in flexural strengthening, a higher bond resistance of the FRP occurs, because the out of plane deformation of the FRP at the initiation of the debonding process is prevented by the strap.

Appendix 5.1-Details on bond-slip relationships and strength models

A5.1.1 EBR systems

A5.1.1.1 Bilinear bond law

A proposal made by one study⁸ for mean and characteristic values of the parameters in the bilinear bond law for different strengthening systems is given in Table A5.1-1.

Table A5.1-1 Parameters of the bilinear T_{6-s} constitutive law for bond

Type		b1	s, (mm)	s _o , (mm)
CFRP strips	Mean value	$0.53\sqrt{f_{cm} \cdot f_{ctm}}$	0.0063	0.21
	5%characteristic value	$0.37\sqrt{f_{cm} \cdot f_{ctm}}$		0.20
CFRP sheets	Mean value	$0.72\sqrt{f_{cm} \cdot f_{ctm}}$	0.0107	0.24
	5%characteristic value	$0.44\sqrt{f_{cm} \cdot f_{ctm}}$	-	0.23

A proposal made by another study⁵ for mean and characteristic values of the bond strength, the maximum slip and the associated fracture energy under the assumption of bilinear bond law is given in Table A5.1-2.

Table A5.1-2 Parameters of the bilinear t,-s constitutive law for bond.

Type	C, (MPa mm)	T, (MPa)	s, (mm)
Strips and sheets	Mean value	$0.25^2 k_b^2 \cdot f_{cm}^{2/3}$	$0.50 k_b^2 \cdot f_{cm}^{2/3}$
	5%characteristic value	$0.17^2 k_b^2 \cdot f_{cm}^{2/3}$	$0.23 k_b^2 \cdot f_{cm}^{2/3}$

A5.1.1.2 Effective bond length

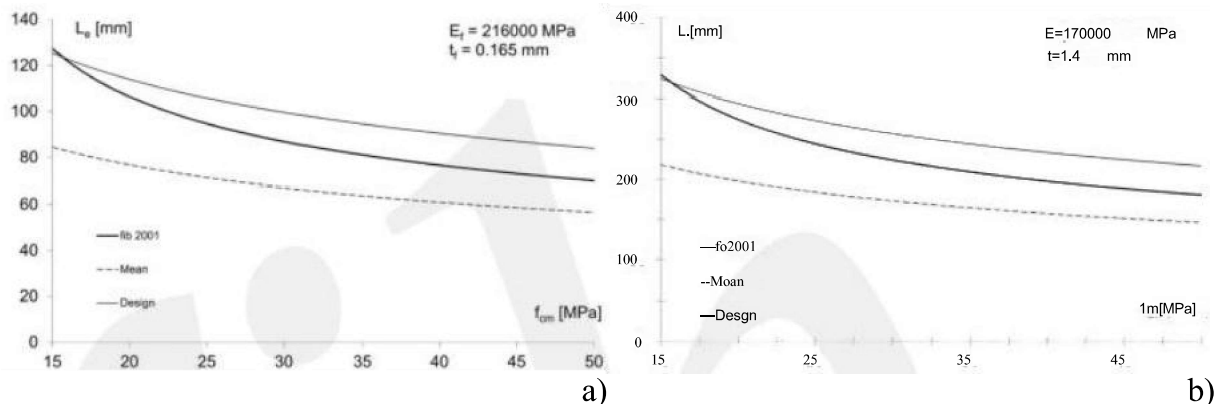


Fig.A5.1-1 Effective bond length for(a)cured in-situ systems and(b)strips

The mean and the design provisions of the effective length [Eqs.(5-7b)and(5-7c)] versus the variation of the concrete strength,are given in Fig.A5.1-1 for a typical cured in-situ system and pre-cured strip,under the assumption of $k_b=1$.The mean provisions are 20 to 30%lower than the characteristic value,depending on the concrete strength.

Fig.A5.1-1 also gives a comparison with the previous formulation in fib³5,showing that the design provisions for the effective length are always safe.

A5.1.1.3 Database on design by testing for debonding at the end anchorage zone

The mean and the 5%characteristic values of the numerical coefficient k (0.25 and 0.17,respectively),used in Eqs(5-11)and(5-12),have been assessed on the basis of a wide experimental database.The experimental results come from more than 280 bond tests⁵on concrete elements strengthened with FRP strips or sheets,with parameters in the following ranges:mean concrete strength 15-62 MPa,elastic modulus of FRP 82-400 GPa,thickness of FRP 0.083-1.6 mm,1-3 layers of sheets,FRP to concrete width ratio 0.15-1.Figure A5.1-2 gives the experimental values of strains at debonding along with the mean and the 5%provisions given by Eqs(5-11)and (5-12),respectively.In the same figure the design provision is also plotted,by dividing the 5%characteristic values by 1.5;the corresponding curve is on the safe side,as all test data are above.Note that strains at debonding are calculated by dividing the debonding strength f_b by the mean elastic modulus E

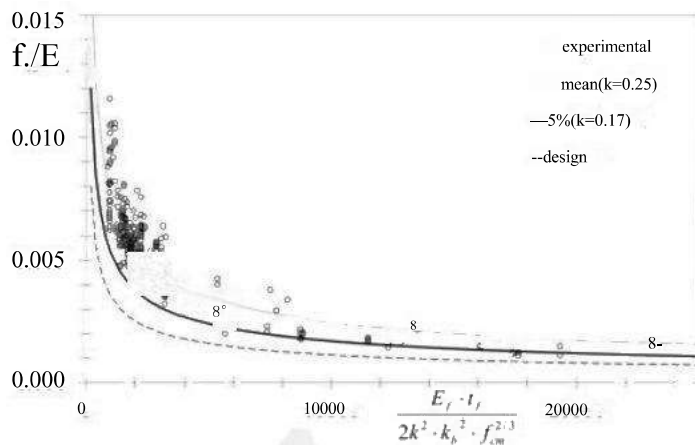


Fig.A5.1-2 Experimental values from bond tests and theoretical provisions for the maximum strain for debonding at the end anchorage zone

A5.1.1.4 Ultimate strength at the end anchorage zone for concrete cover separation

As explained in Section 5.2.1.1, concrete cover separation is initiated by a shear crack at the end of the FRP in combination with the shift in tensile force between the external FRP and the internal rebars. In the presence of internal steel stirrups, the shear crack propagates below the steel stirrups and leads to superficial debonding or to concrete cover separation (see right side of Fig.A5.1-3). On the contrary, without internal steel shear reinforcement shear failure is induced due to the propagation of the diagonal crack along the height of the beam (see left side of Fig.A5.1-3).

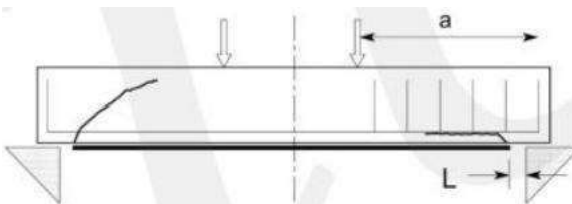


Fig.A5.1-3 FRP end shear failure(left)and FRP end debonding by concrete rip-off (right)

If the concrete cover separation failure load, generally expressed as a critical shear load, is lower than the acting design shear load, this debonding failure can be avoided by providing U-shaped strengthening only at the end of the FRP reinforcement. However, note that irrespective of the flexural strengthening and possible concrete rip-off failure, a shear strengthening verification remains applicable. Indeed, if the shear resistance of the original RC beam is the critical failure load, a suitable shear strengthening should be provided in the full length where it results lower than the design shear load.

The failure load associated with concrete cover separation relates to the shear strength of the concrete, considering the presence of the FRP strengthening in flexure. Several models have been proposed to calculate this shear strength by means of complex and iterative approaches^{36,40}, taking into account a "prestress" effect due to the FRP reinforcement, or simple approaches^{38,42,57,91}. As the contribution of the "prestress" from the FRP reinforcement is generally small⁴², one could arrive at safe predictions by neglecting it. By contrast, the contribution of the internal steel reinforcement to the shear debonding load could be more

relevant. This contribution is expected to be low for small beams and to become higher when the beam dimensions become more realistic. A few of the simple models reported in the literature are summarised next.

The model of Jansze³⁸ provides a simple approach for the concrete cover separation due to the formation of an end critical diagonal crack (see Fig.A5.1-4). The resulting equations are summarised below.

$$Vd \leq VRd = tRb \cdot d \quad (\text{A5-1})$$

where

$$\tau_{Rd} = 0.15^3 \sqrt{3 \frac{d}{a_t} \left(1 + \sqrt{\frac{200}{d}} \right) \sqrt{100 \rho_s \cdot f_{ck}}} \quad (\text{A5-2})$$

$$a_t = \sqrt[4]{\frac{(1 - \sqrt{\rho_s})^2}{\rho_s} d \cdot L^3} \quad (\text{A5-3})$$

$$a > L + d, a < a \quad (\text{A5-4})$$

where L (in mm) is the distance of the FRP end from the support, a (in mm) is the shear span, d (in mm) is the effective depth of the internal steel reinforcement, ρ , is the internal tension steel reinforcement ratio and f is the characteristic value of the concrete compressive strength.

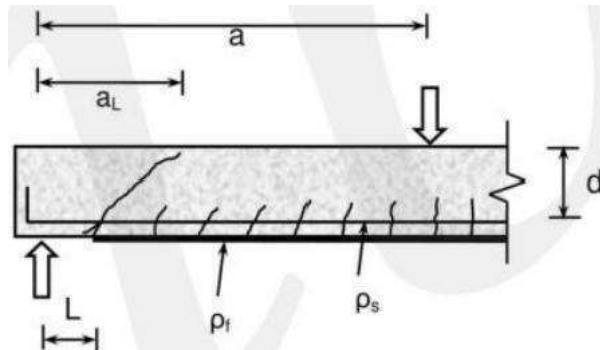


Fig.A5.1-4 Geometrical parameters for the Jansze(1997)model for concrete cover separation

Another simplified and conservative model was proposed by one study⁹¹, in which it is suggested to calculate the design shear force at debonding as:

$$VRd = 1.5 Rdc \quad (\text{A5-5})$$

where $V_{Rd,c}$ is the design shear strength of the concrete beam without the contribution of internal steel reinforcement.

In another study⁴², a more complex model takes into account explicitly the contribution of the internal shear reinforcement by means of an effective strain and the contribution of the FRP reinforcement. Neglecting the latter one as already discussed, the formulation is as follows:

$$V_{Rd} = V_{Rd,c} + \frac{A_s \cdot E_s \cdot \epsilon_{v,e} \cdot d}{s} \quad (\text{A5-6})$$

where A_{st} is the total cross sectional area of the two legs of each stirrup, E is the elastic modulus of steel, d is the effective depth of the internal steel reinforcement, s is the longitudinal spacing of the stirrups and ϵ_e is the effective strain in the internal steel shear reinforcement. A best-fit expression for ϵ_e is given by this study⁴² as follows:

$$\epsilon_{v,e} = \frac{10}{\sqrt{\alpha_{\text{flex}} \cdot \alpha_E \cdot \alpha_t \cdot \alpha_w}} \quad (\text{A5-7})$$

$$\alpha_{\text{flex}} = \frac{(E \cdot I_2) - (E \cdot I_{02})}{(E \cdot I_{02})} \quad (\text{A5-8})$$

$$\alpha_E = \frac{E_f}{E_c} \quad (\text{A5-9})$$

$$\alpha_t = \left(\frac{t_f}{d} \right)^{1.3} \quad (\text{A5-10})$$

$$\alpha_w = \frac{b}{b_f} \leq 3 \quad (\text{A5-11})$$

where $(E \cdot I_2)$ and $(E \cdot I_{02})$ are the flexural stiffnesses of the cracked section with and without FRP reinforcement, respectively. The effective strain is assumed to depend on parameters which are important for flexural debonding because it was observed that shear debonding generally occurs after the formation of a significant shear crack which greatly increases the curvature near the FRP end⁴².

The model adopted in this Bulletin for the verification of concrete cover separation extends on the Jansze³⁸ model, in accordance with DAfStb⁵⁷, and is described in Section 6.3.5.

A5.1.1.5 Database on design by testing for debonding at intermediate cracks

The mean and the 5% characteristic values of the numerical coefficients, $k_{c,r,m}$ and k_c , used in Eqs(5-14) and (5-15) for predicting the maximum strain for debonding at intermediate cracks have been assessed on the basis of a database of 214 results of beams externally reinforced in bending with FRP materials (164 cured in-situ systems and 50 pre-cured strips). For cured in-situ FRP systems, the relevant geometric and mechanical parameters are in the following ranges: concrete width $b=75-960$ mm, FRP width $b=30-480$ mm, $b/b=0.17-1.0$, FRP thickness $t_f=0.11-2.55$ mm, elastic modulus of FRP $E=21-390$ GPa, mean compressive strength of concrete $f_{cm}=21-61$ MPa, mean tensile strength of concrete $f_{ctm}=2.3-4.3$ MPa. For specimens strengthened with pre-cured FRP strips, the key parameters vary in the following ranges: $b=180-800$ mm, $b_f=25-280$ mm, $b/b=0.13-1.0$, $t_f=1.0-6.0$ mm, $E=190-220$ GPa, $f_{cm}=12.6-53.4$ MPa, $f_{ctm}=1.62-4.25$ MPa. Many tests were performed by adopting a four-point bending scheme, though results of three-point bending tests are also present in this database.

Figure A5.1-5 gives the experimental values of strains at debonding along with the mean and the 5% characteristic provisions given by Eqs(5-14) and (5-15), respectively. A design provision is also plotted, by dividing the 5% characteristic values by 1.5. Note that strains at debonding are calculated by dividing the debonding strength f_d by the mean elastic modulus E .

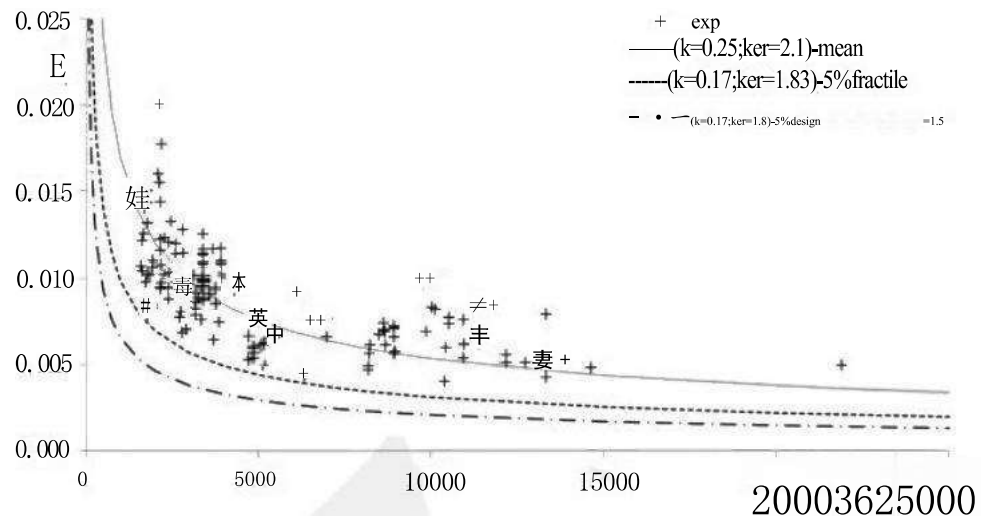


Fig.A5.1-5 Experimental values from beam tests and theoretical provisions for the intermediate debonding strain in EBR systems

A5.1.2 NSM systems

A5.1.2.1 Bond law

A typical experimental t-s relationship for NSM strips is given in Fig.A5.1-6. Up to point B the bond-slip response is nearly linear. The behaviour is mainly influenced by the properties of the strip, the epoxy resin and the geometry of the system. Point B represents the initiation of the nonlinear phenomena leading to a nonlinear relationship between shear stress and slip, and the slip at this point can be interpreted as the one after which the adhesive displays a nonlinear behaviour. The bond strength, t_b , is attained at point C, which is followed by a softening branch as a result of deterioration in the epoxy resin. At point D the adhesive is so damaged that only the embedment in the groove can guarantee any further stress transfer by activating friction mechanisms^{62,67}.

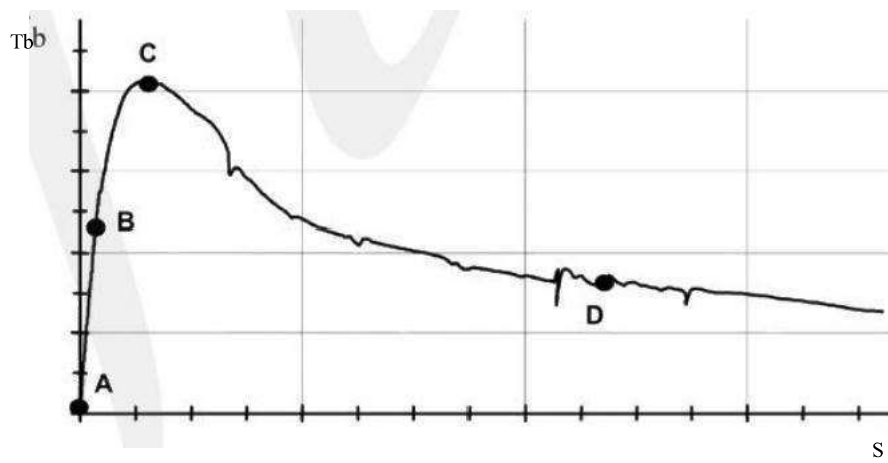


Fig.A5.1-6 Typical experimental bond shear stress-slip relationship for NSM strips

A gradual softening after the peak strength is the case when the bond failure occurs at an interface(epoxy-concrete or bar-epoxy)or when the epoxy cover splitting generated by ribbed bars with low rib protrusions occurs^{8,62}.Indeed, this has been observed in cases

of epoxy-concrete interface failure of round bars^{7,3}, of epoxy cover splitting failure of CFRP ribbed bars³ and of bar-epoxy failure of strips⁸. In these cases a significant amount of post-peak friction develops, due to the interfacial friction or due to the aggregate interlocking effect of the cracked concrete. This bond behaviour can be modelled with a t - s relationship characterised by an initial linear branch followed by a nonlinear one up to the bond strength and by a gradually decreasing branch after the peak value that is asymptotically inclined to a residual strength^{8,7,3} as shown in Fig.A5.1-7a and described by Eq.(A5-12). By using an analytical-numerical strategy for solving the second-order differential Eq.(5-2), when the t - s relationship of Fig.A5.1-7a is used, one study^{9,2} has proved that at the maximum pullout force (Fig.A5.1-7b) a significant portion of the mobilised bonded length is already in the softening phase.

$$t(s) = m \cdot s \quad \text{if } 0 \leq s \leq s_{lin} \quad (\text{A5-12a})$$

$$\tau_b(s) = \tau_{b1} \left(\frac{s}{s_1} \right)^a \quad \text{if } s_{lin} \leq s \leq s_1 \quad (\text{A5-12b})$$

$$\tau_b(s) = \tau_{b1} \left(\frac{s}{s_1} \right)^{-a'} \quad \text{if } s > s_1 \quad (\text{A5-12c})$$

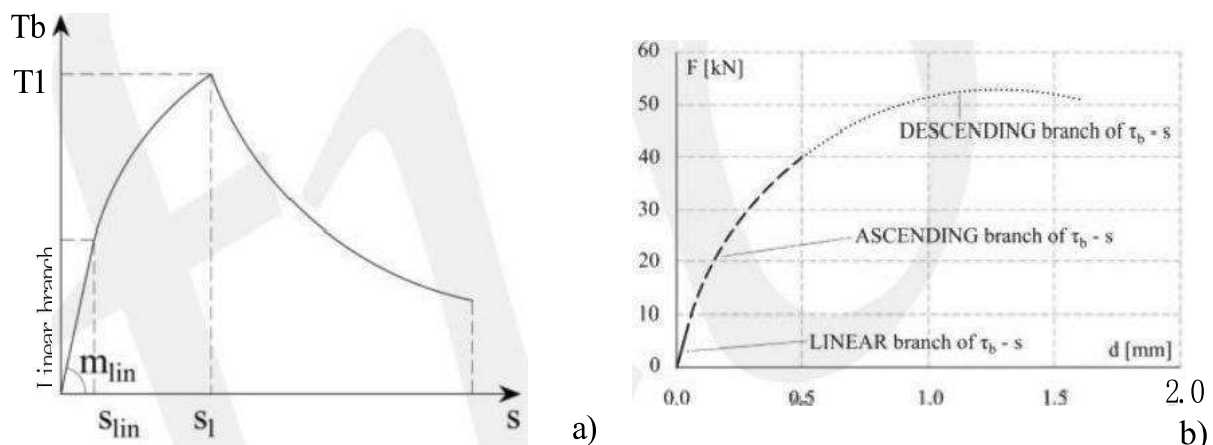


Fig.A5.1-7(a) Local bond stress-slip relationship for NSM FRP in case of interface failure;(b) qualitative correlation between t - s and load-displacement at the loaded end(F - d)relationships in a bond test

Contrary to the above, epoxy cover splitting failure generated by ribbed bars with high rib protrusions or spirally wound bars is of more brittle nature^{6,5,7,3}, characterised by an abrupt decrease in bond stress upon the attainment of the peak strength. However, even after the complete loss of the epoxy cover, a small amount of residual friction remains, since half of the perimeter of the bar is still in contact with the epoxy. In this case the theoretical local bond-slip relationships t - s used for deformed steel bars adjusted with suitable values of coefficients and parameters can be reliably adopted to simulate the experimental bond behaviour of NSM FRP systems (see Fig.A5.1-8 and Eq.A5-13).

$$\tau_b(s) = \tau_{b1} \left(\frac{s}{s_1} \right)^a = C s^a \quad \text{if } 0 \leq s \leq s_1, (0 \leq a \leq 1) \quad (\text{A5-13a})$$

$$t_b(s) = t_b \quad \text{if } s_1 \leq s \leq s_0 \quad (\text{A5-13b})$$

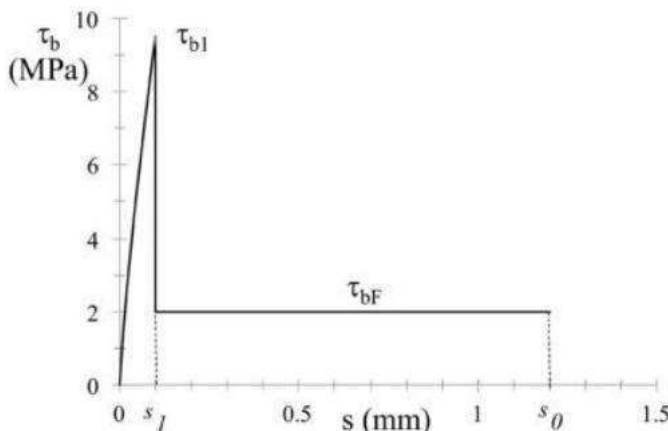


Fig.A5.1-8 Local bond stress-slip relationship for NSM FRP in case of epoxy cover splitting failure

In general, the ultimate slips of bond laws in NSM systems are higher than the respective ones in EBR systems. Test results on bond tests carried out on different NSM systems have evidenced that the local bond-slip law can also be reasonably approximated by a bilinear diagram, as in Fig.5-1, with parameters depending on the axial stiffness, the shape and the surface treatment¹⁵.

The ultimate slip can increase with the roughness of the surface of the FRP, resulting in an increase of the energy absorption capacity. Both the peak shear stress τ_{b1} and the ultimate slip s_0 increase with the decrease of the axial stiffness of the FRP; and the elastic stiffness of the bond law increases as the axial stiffness of the FRP increases.

The surface treatment is expected to be reflected both on the peak value of the shear stress and on the post-peak behaviour: a rougher surface should increase the peak stress and the post-peak behaviour is, in general, more brittle in case of a smooth surface, due to the rapid decay of bond, since the interlocking phenomena are less pronounced.

The ability of most types of NSM FRP reinforcement to transfer shear stresses to the concrete for large relative displacements results in high values of fracture energy G . Hence, unlike for EBR systems, for NSM reinforcement it is generally possible to transfer forces up to the ultimate tensile strength of the FRP materials over a relatively small bond length at a single crack (for bond lengths in the range 150 mm to 200 mm, depending on the elastic modulus of the adhesive).

A5.1.2.2 Database on design by testing for assessing the maximum strain at failure in NSM FRP

An empirical formulation for calculating the maximum strain in the NSM FRP reinforcement is proposed by one study⁸⁴, based on the statistical regression of data from bond tests. A database of 174 test results has been selected, corresponding to different types of bond failure: epoxy-concrete interface failure, epoxy-FRP interface failure, and epoxy splitting. The maximum strain depends on the perimeter of the groove, p_g the elastic modulus E_f , and the area A_f of the FRP, according to the following expression:

$$\varepsilon_{\max,th} = a \frac{\left(\frac{p_g}{E_f \cdot A_f}\right)^c}{(A_f)} \quad (\text{A5-14})$$